ELSEVIER

Journal of Structural Geology 28 (2006) 2011–2022

JOURNAL OF STRUCTURAL GEOLOGY

www.elsevier.com/locate/jsg

Fault reactivation and active tectonics on the fore-arc side of the back-arc rift system, NE Japan

Naoko Kato [a,*], Hiroshi Sato [a], Norihito Umino [b]

[a] *Earthquake Research Institute, The University of Tokyo, 1-1-1 Yayoi, Bunkyo-ku, Tokyo 113-0032, Japan*
[b] *Research Center for Prediction of Earthquakes and Volcanic Eruptions, Graduate School of Science, Tohoku University, Aoba-ku, Sendai 980-8578, Japan*

Received 6 June 2006; received in revised form 30 July 2006; accepted 17 August 2006
Available online 13 October 2006

Abstract

Positive basin inversion is documented using seismic reflection profiles and seismic data on the fore-arc side of the back-arc rift system of northern Honshu, Japan. This finding within a seismically active region is used to understand source fault geometry based on fault reactivation models. Seismic reflection profiles and Bouguer gravity anomalies along with available surface and subsurface evidence define a >300-km-long normal fault system, formed in Miocene time, that bounds the fore-arc side of the Miocene back-arc basin.

Based on the geometry of the seismogenic source fault which was estimated from aftershock distribution and seismic reflection profiles, reverse fault reactivation of former Miocene normal faults occurred and is presently occurring across the entire seismogenic zone. This contractional event began in late Neogene time. The total amount of shortening as inferred from sequential cross section restoration is approx. 20% of the total amount of Miocene extension in the fore-arc side of the northern Honshu. Thus, the overall extensional architecture of the region inherited from Miocene rifting was only slightly modified by the superimposed contractional deformation. Reverse fault reactivation seems to occur only when the dip angle of precursor normal faults is 60° or less. The geometry and evolution of active thrust faults are strongly controlled by fault reactivation processes and are found in conjunction with the development of new thrust faults that propagate across the normal fault footwalls with shortcut trajectories.

Keywords: Fault reactivation; Active and seismogenic faults; Basin inversion; Aftershock distribution; Northern Honshu; Japan

1. Introduction

Estimation of strong ground motion associated with crustal earthquakes provides a base for seismic hazard mitigation. The estimation of strong ground motion requires an understanding of fault parameters such as the deep geometry of source faults (e.g., Irikura, 2002). Unfortunately, most active crustal faults show little seismicity along the fault surface. Direct imaging via the seismic reflection method effectively reveals the deep geometry of source faults before rupture (e.g., Sato et al., 2002a). However, survey costs and the number of target faults necessitate the expansion of source fault models with detailed but regional geologic information.

Fault reactivation processes play an important role in crustal dynamics (e.g., Coward, 1994; Holdswaoth et al., 1997). The development, evolution and reactivation of fault surfaces through time can be quantitatively studied using through analogue and/or numerical modeling. The applicability of the fault reactivation concept must be tested at depth when geologic information is used to construct a source fault model. Most known basin-scale examples of fault reactivation are based on geological evidence or on seismic reflection profiles. Active in situ fault reactivation has been extensively studied as suggested by repeating earthquakes concentrated along major thrust fault in subduction zones (e.g., Igarashi et al., 2003) down to great depth (Wiens and Snider, 2001). However,

* Corresponding author. Fax: +81 3 5689 7234.
E-mail address: naoko@eri.u-tokyo.ac.jp (N. Kato).

0191-8141/$ - see front matter © 2006 Elsevier Ltd. All rights reserved.
doi:10.1016/j.jsg.2006.08.004

systematic investigation along active compressional fault zones that have experienced tectonic inversion is rare. Yet, studies of such fault zones which are associated with crustal scale rupturing may lead to an enhanced understanding of fault reactivation processes.

On July 26, 2003, the Northern Miyagi earthquake (M6.4) occurred along a major basin boundary fault located within the Miocene back-arc rift system in northern Honshu, Japan. This shallow crustal earthquake provides a rare opportunity to investigate in situ the reverse reactivation of a precursor normal fault set during positive tectonic inversion. In this paper we describe in detail the geological structure of the eastern margin of the Northern Honshu rift system (Sato et al., 2004), as inferred from interpretation of seismic reflection profiles and integrated with earthquake data. The study area includes the source area of the Northern Miyagi earthquake. New data obtained through this study provide the constraints to discuss the formation of the back-arc rift basins and in situ compressional inversion processes at depth.

2. Geological setting

Northern Honshu, Japan, is a classic example of a trench-arc–back-arc system. At present, northern Honshu undergoes contraction perpendicular to the NNE–SSW-trending arc as indicated by geodetic measurements, active faults (Active Fault Research Group, 1991) and focal mechanisms (e.g., Hasegawa et al., 2000). Northern Honshu separated from the Eurasian continent during an episode of rifting in early Miocene time (Otofuji et al., 1985). Crustal attenuation of northern Honshu was associated with the opening of the adjacent back-arc basin (Sato, 1994). Since late Neogene time this domain was affected by contractional deformation which led to the development of thrusts and related folds. However, evidence for pre-contractional extension is well preserved in the crustal structure and reveals a systematic attenuation towards the back-arc domain (Iwasaki et al., 2001).

On the fore-arc side of northern Honshu, pre-Neogene rocks consist of a Jurassic accretionary complex locally intruded by Cretaceous granites and extensively crop out in the Kitakami massif. The western margin of the Kitakami massif is marked by a steep Bouguer anomaly gradient (Fig. 1), suggesting a subsided back-arc structure. The distribution of the lower Neogene back-arc sediments is bounded by this gravity anomaly belt; the surface structural expression of the belt corresponds to a west-dipping normal fault system (Kitamura, 1963). The architecture of the normal fault system, as constrained by integrated seismic reflection profiles, gravity data, surface and subsurface geological information, is described in detail in the forthcoming sections.

The family of lower Neogene, largely Miocene extensional structures that stretches for over 300 km along the western margin of the Kitakami massif is here defined as the Kitakami fault system. During the rifting stage, the early Miocene volcanic front was located along the eastern edge of the Miocene rift basins (KFS in Fig. 2; Ohguchi et al., 1989; Tatsumi et al., 1989).

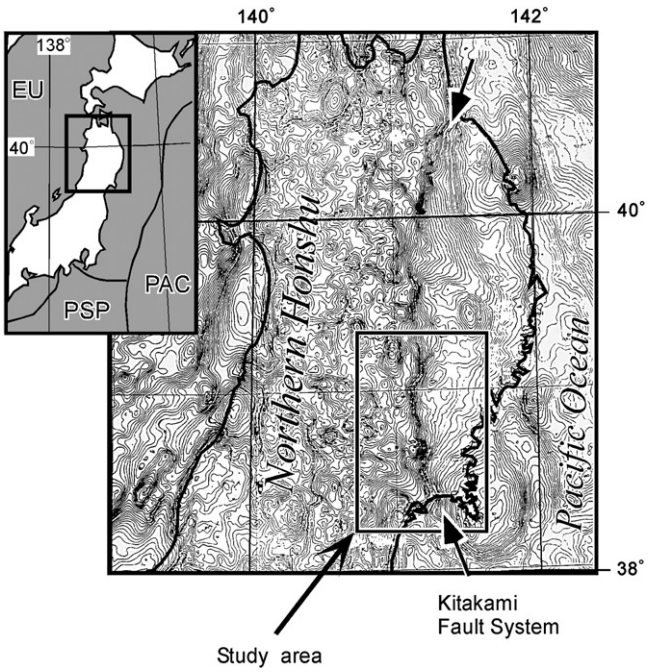

Fig. 1. Bouguer anomaly map of Northern Honshu, Japan, after Komazawa et al. (1999). EU: Eurasian Plate, PAC: Pacific Plate, PSP: Philippine Sea Plate.

The evolution of late Neogene tectonics in northern Honshu can be effectively subdivided in three main stages: (i) a period of widespread extensional deformation of early Miocene age; (ii) a period of relative tectonic quiescence of late Miocene

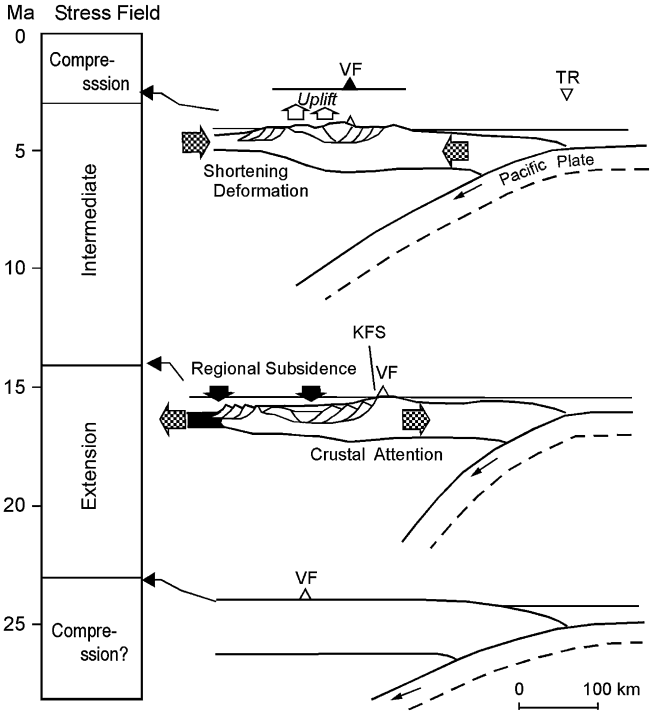

Fig. 2. Neogene tectonic evolution of Northern Honshu modified after Sato and Amano (1991). VF: volcanic front, TR: trench axis, KFS: Kitakami fault system.

age; and (iii) a period of contractional deformation, active since Pliocene time (Fig. 2; Sato and Amano, 1991; Sato, 1994). The direction of the maximum tensional stress during the first, extensional stage, was EW to ENE–WSW, i.e., perpendicular to the arc. During the second stage of tectonic quiescence, a horizontal maximum compressional stress axis was oriented NE–SW, i.e., oblique with respect to the arc. The direction of the maximum compressional stress axis rotated to be perpendicular to the arc again during the third deformation stage (Sato, 1994). As a result of these temporal variations in the orientation and kinematic character of the dominant deformation regime, the back-arc of northern Honshu has experienced an episode of positive inversion (terminology after Williams et al., 1989), from early extension to late contraction, in the Pliocene–Present time interval (Okamura et al., 1995).

3. Basin inversion along the Kitakami fault system

3.1. Ishinomaki area

3.1.1. The 2003 Northern Miyagi earthquake

The series of earthquakes that occurred on July 26, 2003, along the southern part of the Kitakami fault system, which bounds the eastern margin of the Miocene northern Honshu rift system (Sato et al., 2004), had magnitudes ranging between 5.5 and 6.4 (Umino et al., 2003; Fig. 3). The epicenter of the mainshock was located on the southern tip of the NS-trending source fault at a hypocentral depth of 7 km (Okada et al., 2003). The earthquake ruptured along a 12-km-long NS-trending fault zone. The moment tensor solution of the mainshock was a NS-trending reverse slip (Fig. 4). According to the distribution of aftershock *P*-axes, EW-trending and WNW–ESE-trending *P*-axes dominated in the northern portion of source area (Umino et al., 2003), suggesting that the rupture occurred with almost net reverse slip kinematics with a slight additional right-lateral component in the northern part. There were no surface ruptures associated with the earthquakes (Kato et al., 2004).

3.1.2. Geology of the Ishinomaki area

The main geological features of the epicentral area of the 2003 Northern Miyagi earthquake are shown in the map of Fig. 4. Paleozoic and Mesozoic extensively crop out in the Kitakami massif. The western margin of the Kitakami massif is bounded by the W-dipping Sue fault; field evidence and geological data indicate that this structure was active in Miocene time with an extensional kinematic character (Kato et al., 2004). Miocene marine sedimentary rocks are distributed in the western plains and hills (Ishii et al., 1982; Fig. 4). The Miocene basin fill is largely divided into two units: the Matsushima-wan Group (syn-rift sediments) and the Shida Group (post-rift sediments). The Matsushima-wan Group syn-rift sequence consists of volcanics and volcaniclastics, fluvio-lucastrine sediments and interbedded marine sandstone and siltstones (Ishii et al., 1982).

The stratigraphic record of the Sue Hills consists of thick conglomerate and gravel units, clast supported conglomerates (footwall fan facies), and poorly sorted breccias (talus facies). This stratigraphy along with the relationships of these deposits with the local structures indicate that this area experienced fault-controlled subsidence during Miocene time. Palaeo-current directions inferred from clast imbrications within the delta-fan facies of conglomerates and gravels (Fig. 4) indicate for these deposits an easterly provenance.

The Matsushima-wan Group syn-rift clastics are unconformably overlain by post-rift sediments of the Shida Group. These latter sediments mainly consist of shallow marine sandstones. The stratigraphic record of the Ishinomaki area indicates that deposition was mainly controlled by eustatic sea-level changes since middle–late Miocene time. This provides evidence for a stage of relative tectonic quiescence since middle–late Miocene time. Pliocene marine sediments unconformably overlie the lower strata.

The local structure of the Ishinomaki area is dominated by contractional deformations, namely thrusts and associated folds. The Asahiyama Hills occupy the core of a gentle N–S-trending anticline. The eastern limb of this structure contains Pliocene strata and older rocks and defines a flexure that is known in the literature as the Asahiyama flexure. This structure dips east, with an inclination of up to 50°. The results of an integrated tectonic and geomorphological study indicate that the Asahiyama flexure is associated with reverse faulting of late Quaternary age (Ishii et al., 1982).

3.1.3. Seismic profiling

To correlate the source fault with geologic structure, seismic profiling was carried out across the focal area of the Northern Miyagi earthquake (Kato et al., 2004). The seismic source was a single vibroseis truck (IVI Y2400). The length of the seismic line was 12 km and the shot and receiver intervals were 25 m. Seismic signals were recorded using a total of 240 channels. For the wide-angle reflection/refraction analysis, 50 sweeps of the vibroseis truck were recorded using 286 channels.

A refraction analysis of the first arrival time data at seven shot points was carried out. The velocity structure was determined by forward modeling using the 2D ray-tracing method described by Iwasaki (1988), in which travel times of diving waves generated in the model are compared and contrasted with observed first arrivals. The velocity model for the refraction profile is presented in Fig. 5c, together with examples of travel-time curves (Fig. 5a) and ray diagrams (Fig. 5b). The observed travel times are explained within an error of 0.07–0.14 s.

The western part of the profile is covered by thick sedimentary layers with a velocity of 1.6–3.5 km/s. These layers pinch out to the east. At the eastern edge of the Sue Hills, the top of the 3.6 km/s layer discontinuously sinks beneath the eastern plain, where strata of the 3.6 km/s layer are covered by a thin, low velocity (0.6–2.3 km/s) layer.

Seismic reflection data were processed through conventional, common mid-point (CMP) methods, including post-stack migration and depth conversion (Kato et al., 2004). The depth-converted seismic section and its geological interpretation are both shown in Fig. 6. Based on the results of velocity analyses and

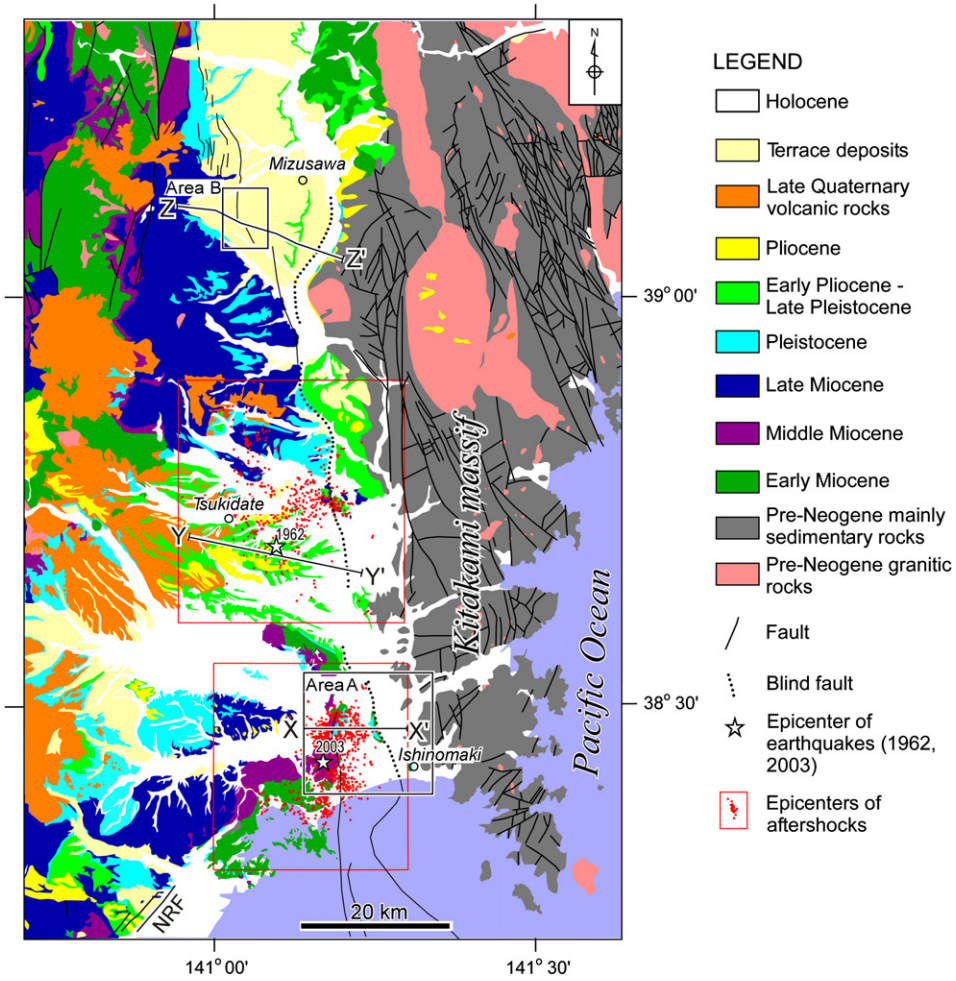

Fig. 3. Geological map of the southern part of the Kitakami river valley, Northern Honshu. The map is modified from the Editorial Committee of Civil Engineering geologic map of Tohoku (1988). NRF: Nagamachi-Rifu fault. Epicenter distribution of aftershocks of the 2003 event is from Umino et al. (2003) and the 1962 event is from Kono et al. (1993).

reflection patterns, the top of the pre-Tertiary basement was interpreted and correlated with horizon D of Fig. 6. This marker horizon is outlined in the seismic profile by relatively large amplitudes and reflected low frequencies.

A density model (Kato et al., 2004) and the local velocity structure indicate that the top of the basement (horizon D) is cut by a step; this is interpreted as the fault that offsets and downthrows the western block under the Sue Hills (CMP 650; Fig. 6). In the fault footwall, the top of the basement (horizon D) occurs at a depth ranging from 100 to 200 m as seen in the easternmost part of the profile (CMP 650–818). The low velocity layer above horizon D and beneath the eastern plain probably consists of Pliocene to Quaternary sediments. In the fault hangingwall, the top of basement is estimated to be at a depth of more than 3 km as seen in the central part of the section (see also Kato et al., 2004). The wedge-shaped part of the section, outlined by poor reflections between horizon C and D (CMP 400–650), is interpreted as a thick fan of conglomerates of the Kakeyama Formation deposited in footwall block at or adjacent to the fault trace; this unit probably was fed by an easterly source and was transported to its present position during the rifting stage (Fig. 7a, b).

The top of the basement (horizon D) is offset and downthrown towards the west with an extensional displacement below the Asahiyama flexure. Faulting resulted in the development of asymmetrical troughs whose geometry is best described in terms of a half-graben architecture. The boundary normal faults were effective in controlling the distribution of clastics within the basin; the main part of the gravel transported from the Kitakami massif was trapped in the eastern half-graben. As a result, the overlying reflective layer directly covers the basement in the western half-graben (Fig. 7a, b).

The shallower part of the profile above horizon C is characterized by coherent reflections. Based on the patterns of reflections in the seismic profile and locally constrained by direct subsurface information from borehole data, the strata below horizon B are interpreted as the syn-rift deposits of the early–middle Miocene Matsushima-wan Group. In contrast, the strata between horizons A and B correspond to post-rift sediments of the middle–late Miocene Shida Group. The base of the Pliocene sediments, whose geometry and position are constrained by direct surface data, is shown as horizon A on the seismic section (Fig. 6).

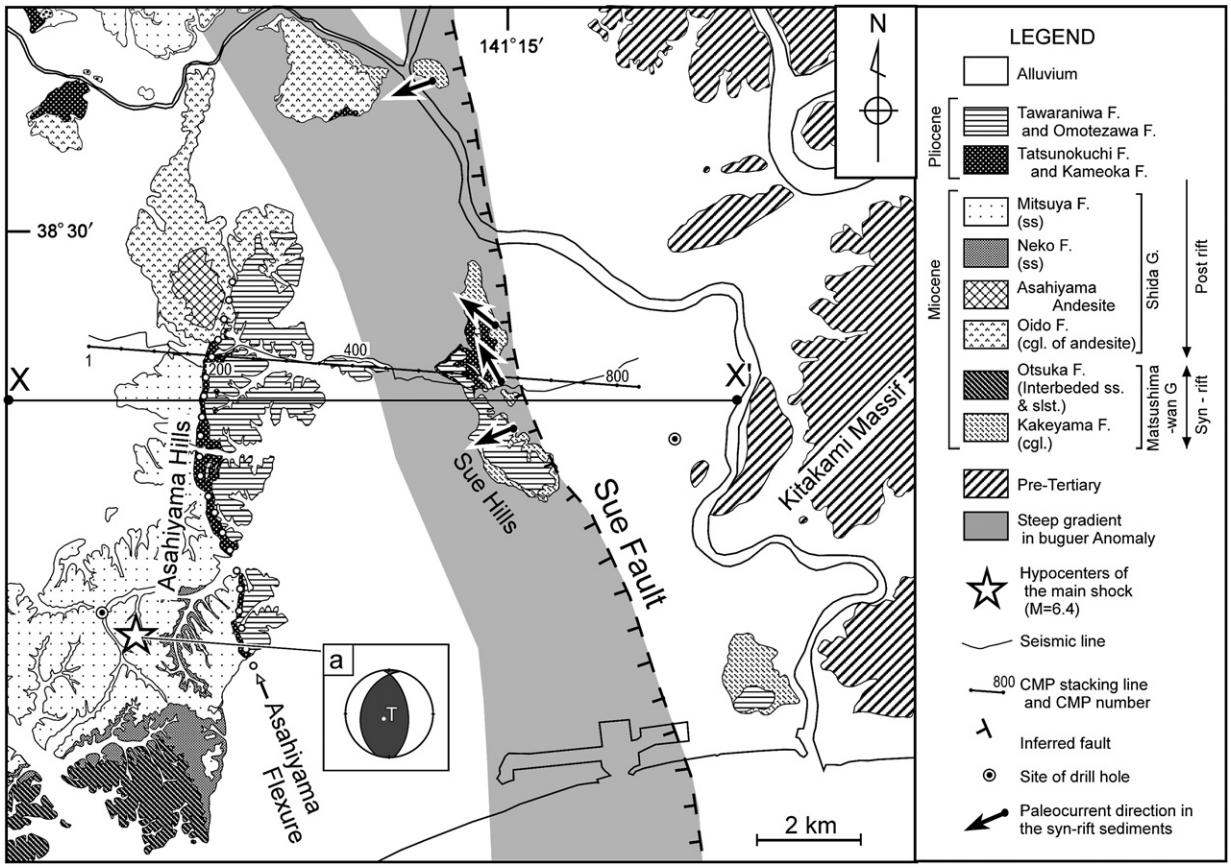

Fig. 4. Generalized geological map of the Ishinomaki area. The map is based on Ishii et al. (1982), Takahashi and Matsuno (1969) and Takizawa et al. (1984). X–X′: see Fig. 7. Litho-facies include cgl, conglomerate; ss, sandstone; slst, siltstone. a: Moment tensor solution of the *M*6.4 mainshock after Okada et al. (2003) and is shown using an equal-area projection onto the lower hemisphere.

3.1.4. Geometry of source faults estimated from aftershock observations

In order to determine the precise location of aftershock hypocenters, a temporary seismic network was installed soon after the occurrence of the *M*6.4 main shock. Thirteen portable data-logger stations and one satellite communication telemetry station were installed in and around the focal area of the *M*6.4 event (Umino et al., 2003).

The hypocenters of aftershocks were estimated through the method of single-event location (Hasegawa et al., 1978) using data observed at portable data-logger stations and those observed at the nearby permanent stations of Tohoku University, National Research Institute for Earth Science and Disaster Prevention (NIED) and Japan Meteorological Agency (JMA). The hypocenters are determined based on P- and S-wave velocity models adopted into the routine procedures of the Tohoku University seismic network (Hasegawa et al., 1978).

The focal depths of aftershocks and focal mechanisms determined by Umino et al. (2003) are illustrated in Fig. 7a. Only aftershocks whose hypocenters have standard deviations less than 1 km are shown. The hypocentral distribution of aftershocks in the depth range of 3–12 km defines the down-dip geometry of the fault surface that ruptured during the *M*6.4 earthquake sequence. The fault surface dips to the west at an angle of ∼50° in the northern part of the aftershock area. As shown in Fig. 7a, the fault surface of the *M*6.4 event revealed by the aftershock distribution is located along the down-dip continuation of the Sue fault at depths ranging from 3 km to 12 km. The frequency distribution of dip angles of the nodal plane of aftershocks shows that the majority of dip angles falls between 40° and 50° in the northern aftershock area (Umino et al., 2003); this inclination is consistent with the dip angle of the source fault estimated from the aftershock distribution. The deepest aftershock focal mechanisms have low-angle nodal planes (Fig. 7a), suggesting a possible low-angle geometry for the main fault near the base of the seismogenic zone.

3.2. Tsukidate area

The Kitakami fault system extends north of the 2003 Northern Miyagi earthquake focal area (Fig. 3), where approx. *M*6.5 (Takemura, 2005) and *M*6.5 earthquakes occurred in 1900 and 1962, respectively. Tohoku University conducted a temporary seismic observation from October 1991 to August 1997 around the focal area of the 1962 *M*6.5 northern Miyagi earthquake, where present seismic activity is relatively high. Four radio telemetry stations were installed; in combination with data from nearby permanent stations of Tohoku University and the JMA, the hypocenters of earthquakes occurring there can be located very precisely. Fig. 7c shows the cross-sectional distribution of

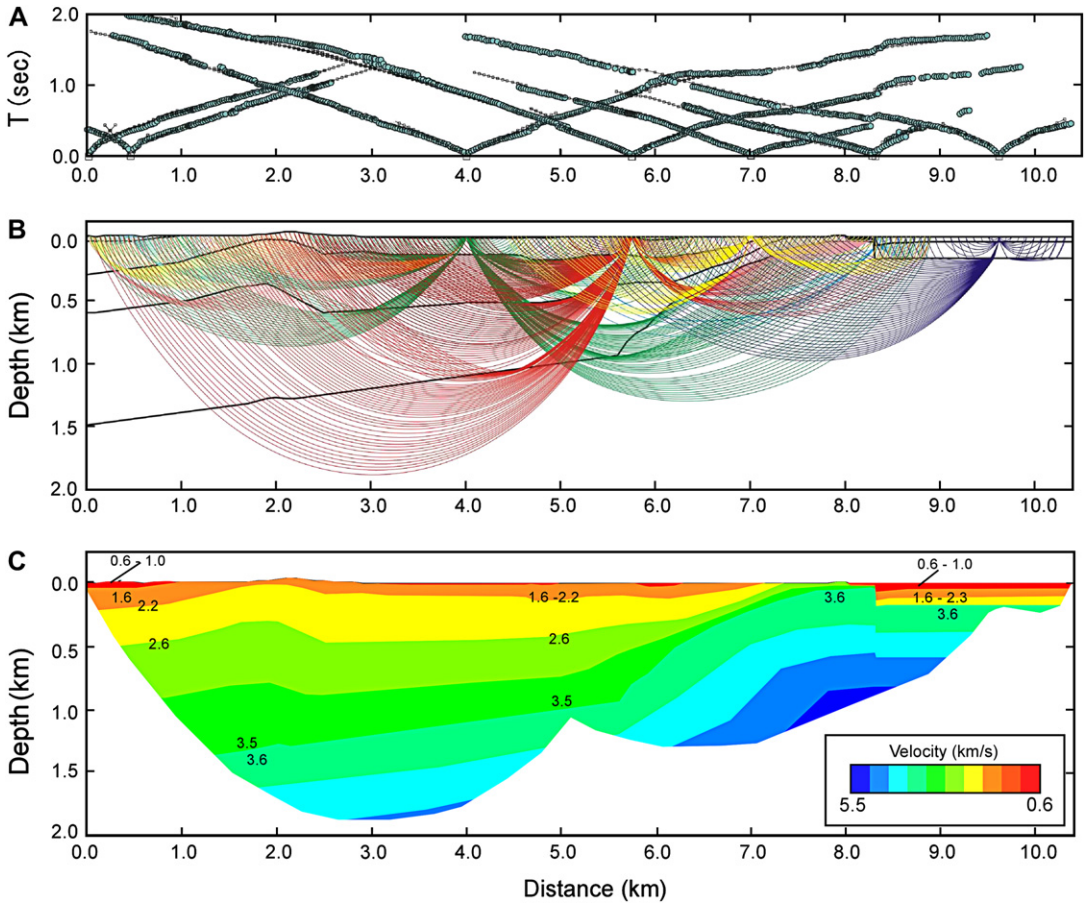

Fig. 5. Velocity model of the Kanan 2003 seismic line obtained by refraction analysis. (a) Comparison between theoretical travel time curves (solid lines) and first arrival data (solid circles). (b) Ray diagrams corresponding to the first arrivals from seven shot points. (c) Velocity model with inferred P-wave velocities (in km/s).

earthquakes along the line Y−Y′ indicated in Fig. 3. Only earthquakes whose hypocenters have standard deviations less than 1.5 km are shown in this figure.

The earthquakes have occurred along a plane dipping westward with inclination of ∼50°. This seismicity consists of the aftershocks of the 1900 and 1962 events. Therefore, the planar distribution of earthquakes reveals the source fault of these *M*6.5 events. Based on the surface information integrated with gravity anomaly data, the previous fault system is that of a normal fault with net extensional displacement. Yet, the

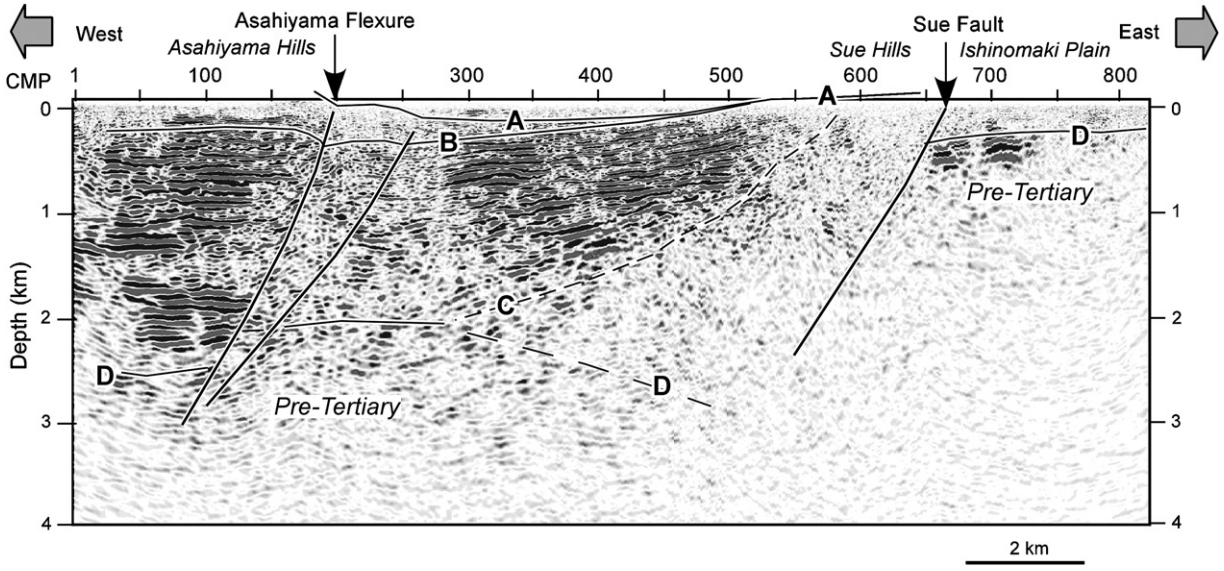

Fig. 6. Post-migrated, depth-converted seismic section of the Kanan 2003 seismic survey and geological interpretation after Kato et al. (2004). V:H = 1:1. A: base of the Kameoka Formation, B: base of the Shida Group, C: boundary between conglomerate facies and stratified facies, and D: upper surface of the pre-Tertiary.

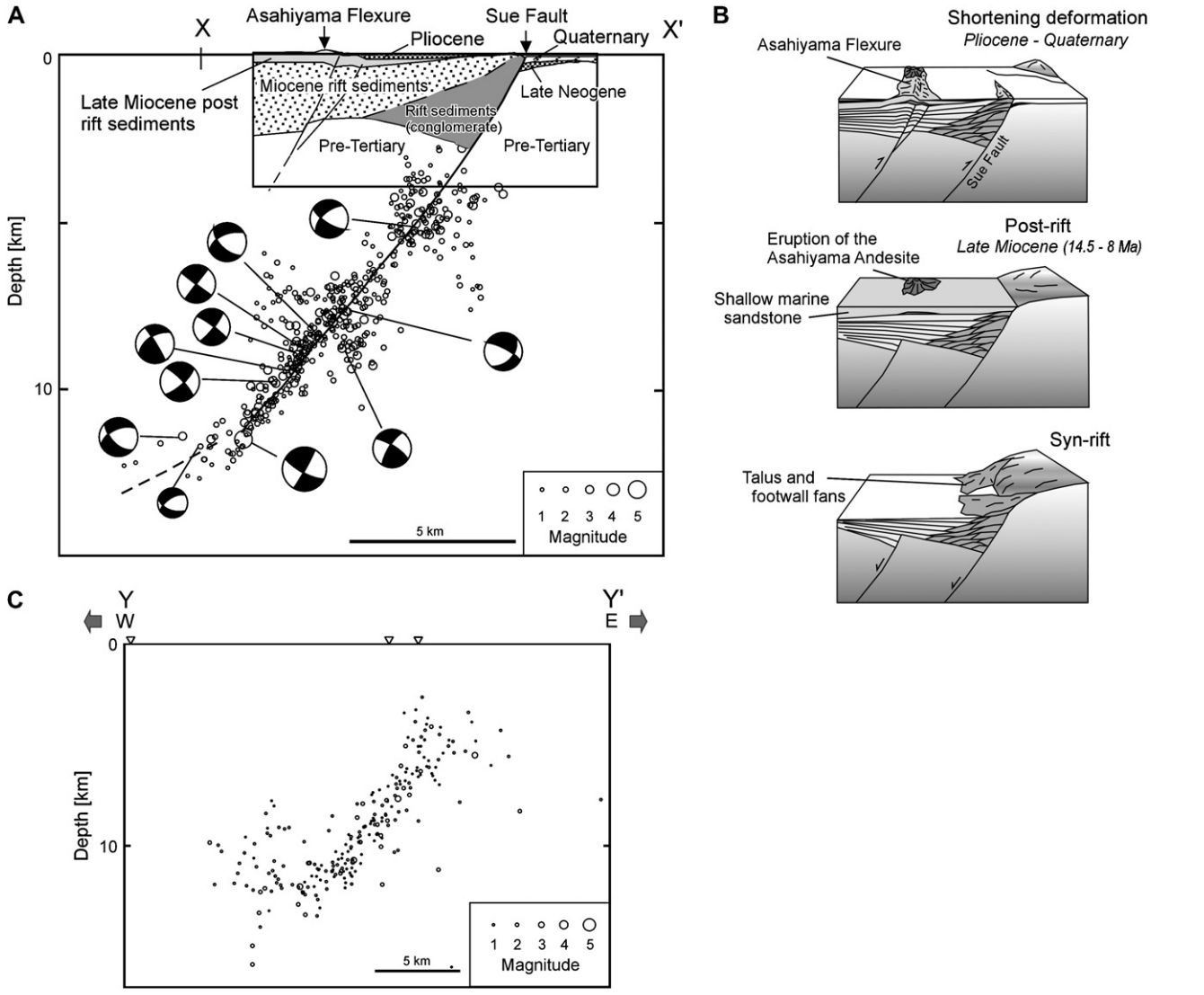

Fig. 7. Schematic diagrams showing the relationship between aftershock distribution and geological structure in the Ishinomaki and Tsukidate areas. (a) Relationship between geological structure and aftershock distribution of the 2003 Northern Miyagi earthquake. Location X–X′ is shown in Figs. 3 and 4. Locations of aftershocks are shown by open circles. Vertical cross section of fault plane solutions of the aftershocks is shown using equal-area projection onto a wall-side hemisphere (after Umino et al., 2003). (b) Schematic diagram showing the basin development. (c) Distribution of earthquakes occurring in the focal area of the 1962 *M*6.5 northern Miyagi earthquake determined by temporary observation data. Locations of earthquakes are shown by open circles. Reverse triangles in the top of the figure denote locations of seismic observation stations. Location of section Y–Y′ is shown in Fig. 3.

fault plane solution of the 1962 Northern Miyagi earthquake shows reverse kinematics (Kono et al., 1993). It seems thus highly probable that the estimated seismogenic source structure was a Miocene basin-bounding normal-fault that was subsequently reverse reactivated. Therefore, as for the 2003 Northern Miyagi earthquake, the 1962 event (*M*6.5) outlines an episode of positive inversion tectonics, where recent compressional deformations were accommodated by reverse reactivation of a precursor Miocene normal fault.

3.3. Mizusawa area

In the Mizusawa area (Fig. 3, Z–Z′), images of a series of west-dipping normal faults were generated using industry seismic reflection sections (JNOC, 2001). The seismic source consisted of four vibroseis trucks (IVI Y2400), with 26 s of 8–70 Hz signals at 40-m intervals. The signal was recorded through a digital telemetry system (JGI, G-daps 4) with 240 channels at 20-m receiver intervals. The post-stacked migrated seismic section of JNOC (2001) was converted from two-way travel times to vertical depths using velocity information derived from reflection moveout analysis (JNOC, 2001) in the Neogene sedimentary unit, integrated with the results of the refraction analysis (Iwasaki et al., 2001) for pre-Neogene basement rocks (Fig. 8a).

An account on the regional geology (Usuta et al., 1986; Kitamura, 1965) indicates that the Neogene sedimentary and abundant volcaniclastic rocks crop out extensively over the study area, whereas the pre-Neogene basement rocks are only found close to the eastern end of the seismic line

(CMP 0–250; Fig. 8b). The lower end of the coherent reflections is interpreted as the base of the basin fill. Three major asymmetrical, normal fault-bounded troughs with characteristic half-graben profile are identified along the seismic section (Fig. 8b). Based on direct sub-surface constraints provided from borehole data (JNOC, 2001), horizon L (Fig. 8b) is here interpreted as the base of the mudstone in the middle Miocene Tsunatori Formation (Kitamura, 1965).

The eastern (F1) and western (Dedana; F2) faults illustrated in the seismic profile of Fig. 8b show evidence for reverse reactivation; this probably occurred at the locations of pre-contractional Miocene normal faults. However, information available for the eastern fault (F1) does not make it possible to document late Quaternary activity. On the other hand, reverse reactivation of late Quaternary age for the Dedana fault (Active Fault Research Group, 1991) is clearly demonstrated by the deformation of recent alluvial fans (Watanabe, 1989; Ikeda et al., 2002). The surface trace of the Dedana fault is deflected to the east near the seismic profile (Fig. 8c), as indicated by the results of an integrated tectonic and geomorphological investigation. A vertical slip-rate of 0.1 mm/year is estimated from the offset of several different river terraces (Active Fault Research Group, 1991).

In cross section, a complex geometrical pattern is observed along the down-dip continuation of the Dedana fault (Fig. 8d). While the structure maintains its overall extensional character at depth, the fault footwall is truncated and slightly offset by a minor reverse fault (indicated as Dfs in Fig. 8b, d) propagating upwards with a shortcut trajectory at a depth <2.5 km. This geometry, i.e., a pre-orogenic normal fault that is reverse reactivated at depth whilst its footwall is trimmed by a superimposed thrust at shallower structural levels, has been widely recognized in well-exposed rift-derived orogens (i.e., the Western Alps; see Gillcrist et al., 1987) and is widely considered a characteristic feature of positive inversion processes (e.g., see Hayward and Graham, 1989, for a comprehensive review). The top of syn-rift deposits (level L of Fig. 8b) is folded both above the tip of the Dedana fault (Dfn in Fig. 8b, d) and above the minor reverse fault in its footwall (Dfs in Fig. 8b, d): these relationships indicate that the Dedana fault itself was also partly reverse reactivated in its shallow structural levels during the upward propagation of the minor reverse fault.

The map trace of this active fault is consistent with the geometry inferred from subsurface information. To the south, the fault trace is deflected eastwards in map view probably due to the formation of the minor thrust in the fault footwall.

The western part of the seismic section is characterized by a distinctive, coherent pattern of seismic reflectors from approx. 13 km (5 s of two-way travel time) which can be traced across the entire profile (Fig. 8a). Similar mid-crustal reflectors at 4.5–5 s of two-way travel time were found in the seismic sections located 20 km north of the Mizusawa area (Sato et al., 2002a). These deeper reflections were correlated to the deeper extension of the E-dipping active fault and interpreted as the mid-crustal detachment at the base of seismogenic layer (Sato et al., 2002a). Similarly, the inferred depth of a major discontinuity outlined in the Mizusawa seismic section (Fig. 8a) also makes it possible to interpret this reflector as a mid-crustal detachment.

In summary, the three examples described in the previous sections and constrained by surface, subsurface and seismic data clearly indicate an episode of positive inversion tectonics in the Miocene Northern Honshu rift system. This episode initiated in Pliocene time and is still active, as outlined by the intense seismicity associated to the investigated faults.

4. Discussion

4.1. Tectonic inversion of a seismogenic source fault

Fault reactivation associated with seismic activity in the continental crust has been studied in many areas, including the New Madrid Seismic Zone (e.g., Mueller and Pujol, 2001), southern California (Rivero et al., 2000), Italy (Vilardo et al., 2003) and Argentina (Kley and Monaldi, 2002). However, in most of these settings, the geometry of the seismogenic source fault is not well constrained by hypocentral distribution due to a general paucity or lack of dense microearthquake or of observations of low seismic activity.

Positive basin inversion along the Kitakami fault system, which bounded the fore-arc side of the northern Honshu rift system in early Miocene time, is demonstrated by the geological structures outlined with integrated seismic sections, sedimentary facies analysis and seismicity. The geometry of 2003 Northern Miyagi earthquake source fault was estimated using dense seismic observations down to 12 km. The estimated dip angle was 50°; this value is common for most observed normal faults and is not far from the ideal dip (60°) for Andersonian normal faults (e.g., Wernicke, 1995). Such high-angle reverse faulting commonly occurs as a result of the compressive reactivation of former normal faults (Sibson, 1990).

In the northern Honshu volcanic arc, deep seismic reflection profiles across the Ou backbone range effectively outline the geometry of an active thrust fault and indicate that this fault continues at depth to merge within subhorizontal reflectors at 4.5–5 s (TWT; Sato et al., 2002a). On September 15th, 1998, an $M5.0$ earthquake occurred by reverse faulting in the deeper portion of the Nagamachi-Rifu fault (Fig. 3, Umino et al., 2002). The dip angle of the mainshock is 30° as inferred from focal mechanism analysis and aftershock distribution. Deep seismic reflection profiling shows that the up-dip continuation of the source fault can be traced to the Nagamachi-Rifu fault. This structure was originally a normal fault in Miocene time that was produced during the same event that led to development of the Kitakami fault system (e.g., Sato et al., 2002b). The focal mechanisms of the 2003 Northern Miyagi earthquake show the low-angle reverse faulting near the base of the seismogenic zone (Fig. 7a). Based on the above-mentioned evidence, the Kitakami fault system is here interpreted as a listric fault system that merges to depth in the seismogenic upper crust.

The interpretation of a general listric fault geometry integrated with the surface, subsurface and seismic data described in this paper provides the grounds for a kinematic

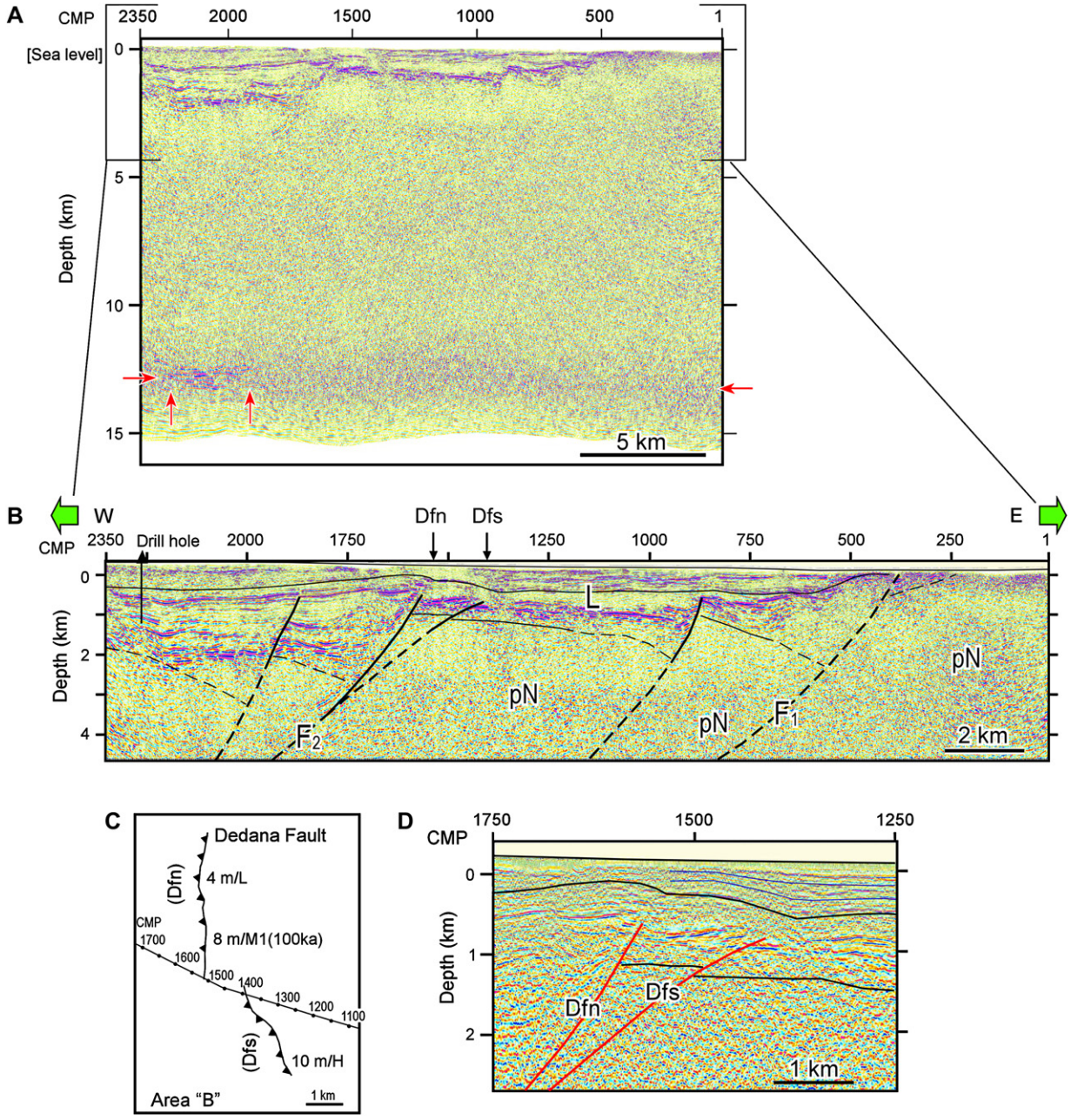

Fig. 8. Seismic reflection profile across the Kitakami river valley in the Mizusawa district. V:H = 1:1 for all seismic sections. (a) Depth-converted seismic section based on JNOC (2001). Location of section Z–Z′ is shown in Fig. 3. Coherent reflectors in the mid-crust are marked by arrows. (b) Geological interpretation of the shallower seismic section. Dfn: northern trace of the Dedana fault, Dfs: southern trace of the Dedana fault, F1, F2: faults, see text. L: probable base of the Tsunatori Formation (middle Miocene), pN: pre-Neogene. (c) The trace of the active fault and the location of the seismic line. The active fault map is after Ikeda et al. (2002). Vertical displacement (m) and marker surface (L, M1, H) are shown. L: lower terrace, M1: middle terrace (100 ka), H: higher terrace. (d) Enlarged seismic section around the Dedana fault.

reconstruction of the Kitakami fault system through time. This was achieved using conventional analysis methods and specific software packages (the 2D Move of Midland Valley) for balanced cross section restoration and forward modeling (Fig. 9). The depth of the mid-crustal detachment was estimated to be at the bottom of the seismogenic zone marked by coherent sub-horizontal reflections at 5 s. (TWT; approx. 13 km in depth). The balanced section and their restored templates which satisfy the geometry of the seismic source fault and rift basins are shown in Fig. 9. The sequential restoration of superposed deformations makes it possible to quantify the amounts of pre-thrusting, syn-rift extension and of post-rift shortening along the section: these are 5.2 km and 1.0 km, respectively (Fig. 9). These values quantitatively illustrate the inferred history of positive tectonic inversion from normal fault development in Miocene time to reverse reactivation in the Pliocene–Present time interval. The restoration of the section, integrated with available surface, subsurface and seismic

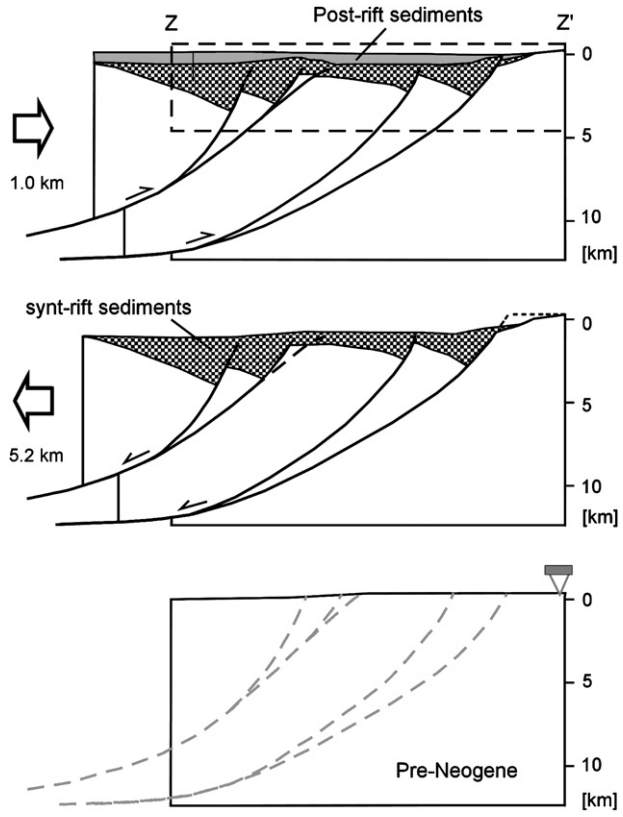

Fig. 9. Balanced geological cross section showing the evolution of the Kitakami fault system in the Mizusawa area. The rectangular boxes near broken line correspond to the seismic section shown in Fig. 8(b). V:H = 1:1.

information, ultimately suggests the possibility of full reactivation of the Miocene normal fault within the whole seismogenic layer.

4.2. Tectonic evolution of the Kitakami fault system

A steep gradient is evident in the Bouguer anomaly along the western edge of the Kitakami massif. Fault reactivation, similar to that described above, is dominant along the fore-arc side of the Miocene rift system. Okamura et al. (1995) described the features of positive basin inversion in the eastern Sea of Japan, where the Miocene normal faulting was associated with the back-arc rifting stage. These authors identified three main phases of fault evolution, namely (i) syn-rift normal faulting, (ii) post-rift tectonic quiescence and (iii) reverse normal fault reactivation during positive inversion.

The same basic deformation history has been confirmed on the fore-arc side of the northern Honshu rift system in this study. Constructed with the interpretation of a listric fault geometry at depth, the balanced cross section of Fig. 9 illustrates quantitatively the history of positive tectonic inversion and makes it possible to estimate the amount of Miocene extension to be approx. 5.2 km in the Mizusawa area. In contrast, the inferred amount of shortening is only approx. 1.0 km. In summary, the relatively mild contractional overprint onto the Mizusawa normal fault system only slightly modified the overall extensional architecture that the basin had developed in Miocene time as a consequence of rifting.

4.3. Significance of 'lock-up' angles in compressional inversion

Investigations on frictional mechanics indicate that reverse reactivation of listric normal faults during positive inversion becomes progressively more difficult towards the upper fault terminations where the fault surfaces steepen (Sibson, 1990). Reverse fault rupturing does not seem to occur when fault dips are >60°, i.e., the predicted 'lock-up' angle for a 'Byerlee' friction coefficient of 0.6 (Sibson and Xie, 1998).

This study documents several examples of reverse reactivation of pre-existing normal faults along the Kitakami fault system. Reverse reactivation combined with the development of new thrust faults which propagated upwards across normal fault footwalls with shortcut trajectories appear to be strongly controlled by the dip angle of pre-existing faults. In the Mizusawa area, two of the four Miocene normal faults were reverse reactivated. The critical dip angle of normal faults that controls reverse reactivation vs. footwall truncation is in excess of 60° (Fig. 8b). In the south, the footwall of the Dedana fault was truncated by a newly formed thrust that propagated upwards with a shortcut trajectory, whereas in the north the Dedana fault was simply reverse reactivated (Fig. 10). The Dedana fault seems to dip approx. 60° in the region of the seismic profile. The dip angle of Dfn, illustrated in Fig. 8d, is close to 60°, the dip of the theoretically estimated 'lock-up' angle (Sibson, 1990). Similarly, in the Ishinomaki area, the dip angle of the fault beneath the Asahiyama flexure is close to 60°; the formation of a newly formed thrust east of the Asahiyama flexure suggests an analogue mechanism that could result in development of a footwall shortcut thrust.

5. Conclusions

Three main conclusions can be drawn from this study:

1. Based on the geometry of the seismogenic source fault identified from aftershock distributions and seismic reflection profiles, reverse fault reactivation of pre-existing Miocene normal faults occurred across the entire seismogenic zone.
2. Analogous to those described in this paper, positive basin inversion processes in the eastern part of the Sea of Japan were also confirmed on the fore-arc side of the failed rift basin. Under the assumption of mid-crustal detachment and listric fault geometry at depth, the total amount of contraction of late Neogene age was approx. 20% of the amount of Miocene extension along the fore-arc side of the Miocene northern Honshu rift system. Thus, the original Miocene extensional architecture, dominant in northern Honshu, was only slightly modified by superimposed thrusting and reverse fault reactivation.
3. Reverse reactivation of pre-existing normal faults seems to occur where the precursor fault surfaces dip 60° or less.

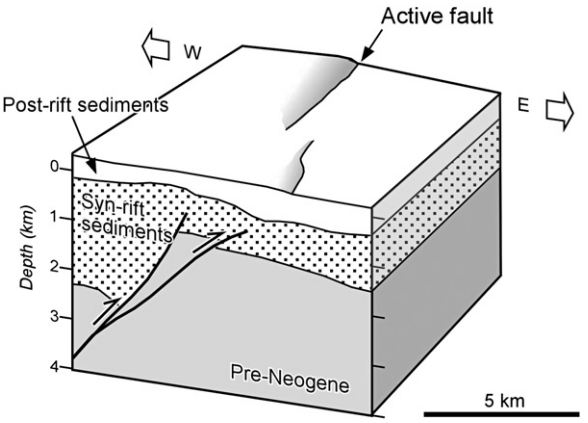

Fig. 10. Schematic 3D block diagram showing the relationship between active fault and footwall short-cut thrust traces.

This provides an original, natural test case for theoretical studies on the mechanics of fault reactivation during tectonic inversion episodes.

Acknowledgements

The authors gratefully acknowledge the Japan Oil, Gas and Metals National Corporation for making seismic data available and allowing for the publication. We are grateful to Takaya Iwasaki for providing the ray-tracing analysis software and to Shin Koshiya, Kenshiro Otsuki and David Okaya for discussion. We also thank Richard H. Sibson, Christophere Wibberley, Enrico Tavarnelli, Rob Butler and Mario Grasso for carefully reviewing the manuscript. Their efforts helped to improve our manuscript. This study was supported by Grants-in-Aid for Scientific Research (14209004, 15800009, 17540431).

References

Active Fault Research Group, 1991. Active Faults in Japan: Sheet Maps and Inventories. In: revised ed (Ed.). University of Tokyo Press, Tokyo, 437 pp. (in Japanese).

Coward, M.P., 1994. Inversion tectonics. In: Hancock, P.L. (Ed.), Continental Deformation. Pergammon Press, Oxford, pp. 280–304.

Editorial Committee of Civil Engineering geologic map of Tohoku, 1988. Civil Engineering Geologic Map of Tohoku, Scale 1:200,000. Japan Institute of Construction Engineering, Tokyo, 461 pp. (in Japanese).

Gillcrist, R., Coward, M.P., Mugnier, J., 1987. Structural inversion and its controls: examples from the Alpine foreland and the French Alps. Geodinamica Acta 1, 5–34.

Hasegawa, A., Umino, N., Takagi, A., 1978. Double-planed structure of the deep seismic zone in the northeastern Japan arc. Tectonophysics 47, 43–58.

Hasegawa, A., Yamamoto, A., Umino, N., Miura, A., Horiuchi, A., Zhao, D., Sato, H., 2000. Seismic activity and deformation process of the overriding plate in the northeastern Japan subduction zone. Tectonophysics 319, 225–239.

Hayward, A.B., Graham, R.H., 1989. Some geometrical characteristics of inversion. In: Cooper, M.A., Williams, G.D. (Eds.), Inversion Tectonics. Special Publication 44. Geological Society of London, pp. 17–39.

Holdswaoth, R.E., Bulter, C.A., Roberts, A.M., 1997. The recognition of reactivation during continental deformation. Journal of Geological Society, London 154, 73–78.

Igarashi, T., Matsuzawa, T., Hsegawa, A., 2003. Repeating earthquakes and interplate seismic slip in the northeastern Japan subduction zone. Journal of Geophysical Research 108, doi:10.1029/2002JB001920.

Ikeda, Y., Imaizumi, T., Togo, M., Hirakawa, K., Miyauchi, T., Sato, H. (Eds.), 2002. Atlas of Quaternary Thrust Faults in Japan. University of Tokyo Press, Tokyo, 254 pp. (in Japanese).

Irikura, K., 2002. Recipe for estimating strong ground motions from active fault earthquakes. In: Fujinawa, Y., Yoshida, A. (Eds.), Seismotectonics in Convergent Plate Boundary. Terrapub, Tokyo, pp. 45–55.

Ishii, T., Yanagisawa, Y., Yamaguchi, S., Sangawa, A., Matsuno, K., 1982. Geology of the Matsushima district, with Geological Sheet Map, scale 1:50,000. Geological Survey of Japan, 121 pp. (in Japanese with English abstract).

Iwasaki, T., 1988. Ray-tracing program for study of velocity structure by ocean bottom seismographic profiling. Zisin 41, 263–266 (in Japanese).

Iwasaki, T., Kato, W., Moriya, T., Hasemi, A., Umino, N., Okada, T., Miyashita, K., Mizogami, T., Takeda, T., Sekine, S., Matsushita, T., Tashiro, K., Miyamachi, H., 2001. Extensional structure in northern Honshu Arc as inferred from seismic refraction/wide-angle reflection profiling. Geophysical Research Letters 28, 2329–2332.

JNOC, 2001. Report on basic geophysical exploration in onshore area, "Mizusawa". Japan National Oil Corporation, 86 (in Japanese).

Kato, N., Sato, H., Imaizumi, T., Ikeda, Y., Okada, S., Kagohara, K., Kawanaka, T., Kasahara, K., 2004. Seismic reflection profiling across the source fault of the 2003 northern Miyagi earthquake (*Mj* 6.4), NE Japan: basin inversion of Miocene back-arc rift. Earth Planets Space 56, 1255–1261.

Kitamura, N., 1963. Tertiary tectonic movements of the green tuff area. Fossils (Kaseki) 5, 123–137 (in Japanese).

Kitamura, N., 1965. Geology of the Yakeishidake district, with Geological Sheet Map, scale 1:50,000. Geological Survey of Japan, 48 (in Japanese with English abstract).

Kley, J., Monaldi, C.R., 2002. Tectonic inversion in the Santa Barbara System of the central Andean foreland thrust belt, northwestern Argentina. Tectonics 21, 1061, doi:10.1029/2002TC902003.

Komazawa, M., Hiroshima, T., Ishihara, T., Murata, Y., Yamazaki, T., Joshima, M., Makino, M., Morijiri, R., Shichi, R., Kishimoto, K., Kikawa, E., 1999. 1:1,000,000 Gravity Map of Japan (Bouguer anomalies). Geological Society of Japan, Tsukuba, 14 (in Japanese with English abstract).

Kono, T., Nida, K., Matsumoto, S., Horiuchi, S., Okada, T., Kaihara, K., Hasegawa, A., Hori, S., Umino, N., Suzuki, M., 1993. Microearthquake activity in the focal area of the 1962 Northern Miyagi Earthquake (M6.5). Zisin 46, 85–93 (in Japanese with English abstract).

Mueller, K., Pujol, J., 2001. Three-dimensional geometry of the Reelfoot blind thrust: implications for moment release and earthquake magnitude in the New Madrid. Bulletin of the Seismological Society of America 91, 1563–1573.

Ohguchi, T., Yoshida, T., Okami, K., 1989. Historical change of Neogene and Quaternary volcanic field in the Northeast Honshu Arc, Japan. Memoirs of the Geological Society of Japan 32, 431–455 (in Japanese with English abstracts).

Okada, T., Umino, N., Hasegawa, A., 2003. Rupture process of the July 2003 northern Miyagi earthquake sequence, NE Japan, estimated from double-difference hypocenter locations. Earth Planets Space 55, 741–750.

Okamura, Y., Watanabe, M., Morijiri, R., Satoh, M., 1995. Rifting and basin inversion in the eastern margin of the Japan Sea. Island Arc 4, 166–181.

Otofuji, Y., Matsuda, T., Noda, S., 1985. Paleomagnetic evidence for Miocene counter-clockwise rotation of Northeast Japan—rifting process of the Japan arc. Earth and Planetary Science Letters 75, 265–277.

Rivero, C., Shaw, J.H., Mueller, K., 2000. Oceanside and Thirtymile Bank blind thrusts: Implication for earthquake hazards in coastal southern California. Geology 28, 891–894.

Sato, H., 1994. The relationship between late Cenozoic tectonic events and stress field and basin development in northeast Japan. Journal of Geophysical Research 99, 22261–22274.

Sato, H., Amano, K., 1991. Relationship between tectonics, volcanism, sedimentation and basin development, Late Cenozoic, central part of northern Honshu, Japan. Sedimentary Geology 74, 323–343.

Sato, H., Hirata, N., Iwasaki, T., Matsubara, M., Ikawa, T., 2002a. Deep seismic reflection profiling across the Ou Backbone Range, northern Honshu Island, Japan. Tectonophysics 355, 41–52.

Sato, H., Imaizumi, T., Yoshida, T., Ito, H., Hasegawa, A., 2002b. Tectonic evolution and deep to shallow geometry of Nagamachi-Rifu active fault system, NE Japan. Earth Planets Space 54, 1039–1043.

Sato, H., Yoshida, T., Iwasaki, T., Sato, T., Ikeda, Y., Umino, N., 2004. Late Cenozoic tectonic development of the back arc region of central northern Honshu, Japan, revealed by recent deep seismic profiling. Journal of Japanese Association for Petroleum Technology 96, 145–154 (in Japanese with English abstract).

Sibson, R.H., 1990. Rupture nucleation on unfavorably oriented faults. Bulletin of the Seismological Society of America 80, 1580–1604.

Sibson, R.H., Xie, G., 1998. Dip range for intracontinental reverse fault ruptures: truth not stranger than friction? Bulletin of the Seismological Society of America 88, 1014–1022.

Takahashi, H., Matsuno, K., 1969. Geology of the Wakuya district, with Geological Sheet Map, scale 1:50,000. Geological Survey of Japan, Tsukuba, 26 (in Japanese with English abstract).

Takemura, M., 2005. Re–evaluation of magnitude and forcal region of the 1900 Northern Miyagi prefecture earthquake in Japan. Zisin 58, 41–53 (in Japanese with English abstract).

Takizawa, F., Kambe, N., Kubo, K., Hata, M., Sangawa, A., Katada, M., 1984. Geology of the Ishinomaki district, with Geological Sheet Map, scale 1:50,000. Geological Survey of Japan, Tsukuba, 103 (in Japanese with English abstract).

Tatsumi, Y., Otofuji, Y., Matsuda, T., Nohda, S., 1989. Opening of the sea of Japan back-arc basin by asthenospheric injection. Tectonophysics 166, 317–329.

Umino, N., Okada, T., Hasegawa, A., 2002. Foreshock and aftershock sequence of the 1998 M 5.0 Sendai, Northeastern Japan, earthquake and its implications for earthquake nucleation. Bulletin of the Seismological Society of America 92, 2465–2477.

Umino, N., Okada, T., Nakajima, J., Hori, S., Kono, T., Nakayama, T., Uchida, N., Shimizu, J., Suganomata, J., Gamage, S., Hasegawa, A., Asano, Y., 2003. Hypocenter and focal mechanism distributions of aftershocks of July 26 2003 M6.4 northern Miyagi, NE Japan, earthquake revealed by temporary seismic observation. Earth Planets Space 55, 719–730.

Usuta, M., Taguchi, K., Okamoto, K., Kitamura, N., 1986. Geology of transect No. 19. In: Kitamura, N. (Ed.). Geology of NE Honshu Arc, Hobundo, Sendai, p. 15 (in Japanese).

Vilardo, G., Nappi, R., Petti, P., Ventura, G., 2003. Fault geometries from the space distribution of the 1990–1997 Sannio-Benevento earthquakes: inference on the active deformation in Southern Apennines. Tectonophysics 263, 259–271.

Watanabe, M., 1989. Complementary distributions of active faults and Quaternary volcanoes, and tectonic movements, along the volcanic front of Northeast Japan. Bulletin of the Department Geography, The University of Tokyo 21, 37–74.

Wernicke, B., 1995. Low-angle normal faults and seismicity: a review. Journal of Geophysical Research 100, 20159–20174.

Wiens, D.A., Snider, N.O., 2001. Repeating deep earthquakes: evidence for fault reactivation at great depth. Science 293, 1463–1466.

Williams, G.D., Powell, C.M., Cooper, M.A., 1989. Geometry and kinematics of inversion tectonics. In: Cooper, M.A., Williams, G.D. (Eds.), Inversion Tectonics. Special Publication 44. Geological Society of London, pp. 3–15.